

Nonlinear interactions in electrophoresis of ideally polarizable particles

David Saintillan^{a)}

Department of Mechanical Science and Engineering, University of Illinois at Urbana-Champaign, Urbana, Illinois 61801, USA

(Received 15 February 2008; accepted 14 April 2008; published online 24 June 2008)

In the classical analysis of electrophoresis, particle motion is a consequence of the interfacial fluid slip that arises inside the ionic charge cloud (or Debye screening layer) surrounding the particle surface when an external field is applied. Under the assumptions of thin Debye layers, weak applied fields, and zero polarizability, it can be shown that the electrophoretic velocity of a collection of particles with identical zeta potential is the same as that of an isolated particle, unchanged by interactions [L. D. Reed and F. A. Morrison, "Hydrodynamic interaction in electrophoresis," *J. Colloid Interface Sci.* **54**, 117 (1976)]. When some of these assumptions are relaxed, nonlinear effects may also arise and result in relative motions. First, the perturbation of the external field around the particles creates field gradients, which may result in nonzero dielectrophoretic forces due to Maxwell stresses in the fluid. In addition, if the particles are able to polarize, they can acquire a nonuniform surface charge, and the action of the field on the dipolar charge clouds surrounding them drives disturbance flows in the fluid, causing relative motions by induced-charge electrophoresis. These two nonlinear effects are analyzed in detail in the prototypical case of two equal-sized ideally polarizable spheres carrying no net charge, using accurate boundary-element simulations, along with asymptotic calculations by the method of twin multipole expansions and the method of reflections. It is found that both types of interactions result in significant relative motions and can be either attractive or repulsive depending on the configuration of the spheres. © 2008 American Institute of Physics. [DOI: 10.1063/1.2931689]

I. INTRODUCTION

Electrokinetic phenomena provide an efficient means of manipulating particles at the microscale.^{1–6} The simplest and most classical of these phenomena is electrophoresis,¹ which describes the motion of a charged particle in an electrolyte when an external electric field \mathbf{E}_0 is applied. The mechanism for this motion has been studied extensively and is well understood: the charged particle attracts counterions in the solution, which accumulate near its surface and form a charge cloud or Debye screening layer. The action of the electric field on the excess charge in this layer then results in the motion of the fluid relative to the particle surface and, therefore, in the propulsion of the particle. In situations where the Debye layer is thin with respect to the particle dimensions, this effect can be modeled using an effective slip velocity at the outer edge of the Debye layer (which effectively coincides with the particle surface in the thin-layer case),

$$\mathbf{u}_s(\mathbf{x}) = -\frac{\varepsilon\zeta}{\mu}\mathbf{E}(\mathbf{x}), \quad (1)$$

where ε and μ denote the electric permittivity and the viscosity of the suspending fluid, ζ is the particle zeta potential (which is a constant material property related to the particle surface charge), and \mathbf{E} is the value of the local electric field on the particle surface. Equation (1) constitutes an effective boundary condition to be used for solving the flow problem

around the particle, from which the electrophoretic velocity can then be inferred as $\mathbf{U} = (\varepsilon\zeta/\mu)\mathbf{E}_0$.

When several particles with the same fixed zeta potential are present in the fluid (as in a suspension), Eq. (1) still applies on the surface of each of them, and it can be shown that the velocity of each particle is the same as if it were isolated, unchanged by interactions.^{7,8} In particular, relative motions will not occur. Consequences of this observation are that (i) electrophoresis in solution is inefficient at separating particles by size (however, separation can be achieved if the particles are placed in a gel⁹), and (ii) hydrodynamic dispersion is not expected to occur in suspensions undergoing electrophoresis.

The classical analysis outlined above, however, neglects two types of nonlinear electrokinetic effects, which as shown here may also arise and result in relative motions in particulate suspensions. The first effect is similar in nature to dielectrophoresis (DEP) (or motion of a particle in a nonuniform electric field) and is a consequence of the Maxwell stress tensor in the fluid,

$$\boldsymbol{\Sigma}^m = \varepsilon(\mathbf{E}\mathbf{E} - \frac{1}{2}E^2\mathbf{1}), \quad (2)$$

which upon surface integration allows the calculation of the electric force and torque on a particle. In the case of a single spherical particle in a uniform field, the electric force and torque are easily shown to be zero. However, when more than one particle are present, the distortion of the external field by the particles may result in nonzero forces by symmetry breaking.¹⁰ A similar observation was previously made by Yariv,¹¹ who considered the case of a single sphere in the

^{a)}Electronic mail: dstn@uiuc.edu.

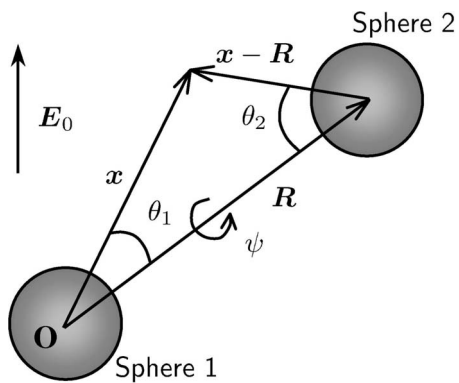


FIG. 1. Problem geometry. We consider two equal-sized spheres of radius a separated by a vector \mathbf{R} and placed in an external electric field \mathbf{E}_0 .

vicinity of a planar wall and showed that the presence of the wall indeed results in a nonzero force. It should be noted that the DEP forces described here are not contingent upon particle polarizability.¹¹

A second effect arises when the particles can polarize under the action of the external field. In this case, they acquire a nonuniform surface charge upon polarization (in addition to their native surface charge or zeta potential), which drives an additional flow around their surfaces. This induced-charge electrophoresis (ICEP) was first predicted in the Ukrainian literature^{12–16} (as reviewed by Murtsovkin¹⁷) and recently rediscovered by Squires and Bazant in the case of isolated spherical particles,^{18,19} as well as nonspherical particles.^{20–24} This effect was also recently observed experimentally.^{25–27} When several particles are present in suspension, these induced flows may result in relative motions through hydrodynamic interactions. While a detailed study of these motions was recently performed in the case of rodlike particles based on slender-body theory,^{22,23} the case of spheres has received less attention, and only asymptotic results valid for very widely separated particles have been proposed so far.^{10,14–16}

In this paper, these nonlinear interactions are analyzed in detail in the prototypical case of two equal-sized spheres. We employ boundary-element simulations, together with asymptotic calculations using the method of reflections^{28,29} and the method of twin multipole expansions,^{30,31} to provide the first highly accurate calculation of the forces and motions resulting from both DEP and ICEP, in the case where the two spheres are ideally polarizable (such as conducting). The governing equations for the electric and flow problems are described in Sec. II, and the boundary integral formulation and results from the calculations are presented in Sec. III. We discuss the implications of these results on particle motions and far-field fluid flow in Sec. IV and conclude in Sec. V.

II. PROBLEM FORMULATION

We consider two neutrally buoyant spheres ($\alpha=1,2$) of radius a suspended in an electrolyte of viscosity μ and electric permittivity ε , as depicted in Fig. 1. We denote by \mathbf{x}_α^c the position of the center of sphere α and by $\mathbf{R}=\mathbf{x}_2^c-\mathbf{x}_1^c$ the separation vector between the two sphere centers, pointing from

sphere 1 toward sphere 2. Both spheres are assumed to be ideally polarizable, as would be the case for conducting particles, and to carry no net charge ($Q_\alpha=0$). This allows us to isolate the nonlinear effects of DEP and ICEP; if the particle charge were nonzero, the standard linear electrophoretic motion could simply be added to the results derived here.

A uniform electric field \mathbf{E}_0 is applied, and under the action of the field, the spheres polarize and attract counterions in the electrolyte, which accumulate near their surfaces leading to the formation of dipolar charge clouds. At steady state, the resulting Debye layers on the particle surfaces repel the local electric field lines, in such a way that the spheres and their charge clouds behave like insulators.¹⁹ In the limit of thin Debye layers and weak applied fields, the electric potential $\phi(\mathbf{x})$ in the electrolyte satisfies Laplace's equation,

$$\nabla^2 \phi(\mathbf{x}) = 0, \quad (3)$$

subject to a no-flux boundary condition at the outer edge of the Debye layers,

$$\begin{aligned} \mathbf{n}_\alpha \cdot \nabla \phi &= 0, \quad \mathbf{x} \in S_\alpha, \\ \phi &\rightarrow -\mathbf{x} \cdot \mathbf{E}_0, \quad |\mathbf{x}| \rightarrow \infty, \end{aligned} \quad (4)$$

where \mathbf{n}_α is the outward normal on the surface S_α of sphere α . In the thin Debye layer limit, the no-flux boundary condition can effectively be applied at the surface of the spheres. Note that this boundary condition can be justified using asymptotic theory.¹⁹ A method of solution of Eq. (3) is described in Sec. III A.

Knowledge of the potential ϕ allows the determination of the electric field $\mathbf{E}=-\nabla\phi$, from which the Maxwell stress tensor can be calculated using Eq. (2). The DEP forces and torques on the particles are then obtained as

$$\mathbf{F}_\alpha = \int_{S_\alpha} (\boldsymbol{\Sigma}^m \cdot \mathbf{n}_\alpha) dS_\alpha, \quad (5)$$

$$\mathbf{T}_\alpha = \int_{S_\alpha} (\mathbf{x} - \mathbf{x}_\alpha^c) \times (\boldsymbol{\Sigma}^m \cdot \mathbf{n}_\alpha) dS_\alpha. \quad (6)$$

It is easy to see that for spherical particles, $\mathbf{T}_\alpha=\mathbf{0}$. Indeed, since the electric field is tangential on the sphere surfaces ($\mathbf{E} \cdot \mathbf{n}_\alpha=0$), the Maxwell stresses on the surfaces are normal: $\boldsymbol{\Sigma}^m \cdot \mathbf{n}_\alpha = -\varepsilon E^2 \mathbf{n}_\alpha / 2$. Observing that $\mathbf{x} - \mathbf{x}_\alpha^c = a \mathbf{n}_\alpha$ on sphere α , we conclude that the dielectrophoretic torque is identically zero.

Finally, the action of the electric field on the nonuniform charge clouds leads to the motion of the counterions near the particle surfaces and drives a steady fluid flow. As shown by Squires and Bazant,¹⁹ this ICEP flow can be captured via an effective fluid slip velocity on the surface of the spheres,

$$\mathbf{u}_s(\mathbf{x}) = -\frac{\varepsilon \zeta(\mathbf{x})}{\mu} \mathbf{E}(\mathbf{x}), \quad \mathbf{x} \in S_\alpha. \quad (7)$$

The effective zeta potential $\zeta(\mathbf{x})$ is now nonuniform and is related to the electric potential drop across the Debye layer,

$$\zeta(\mathbf{x}) = \phi_0^{(\alpha)} - \phi(\mathbf{x}), \quad \mathbf{x} \in S_\alpha, \quad (8)$$

where the constant $\phi_0^{(\alpha)}$ is determined to enforce the neutrality condition on sphere α ,

$$\int_{S_\alpha} \zeta(\mathbf{x}) dS_\alpha = 0, \quad (9)$$

i.e.,

$$\phi_0^{(\alpha)} = \frac{1}{4\pi a^2} \int_{S_\alpha} \phi(\mathbf{x}) dS_\alpha. \quad (10)$$

The fluid velocity $\mathbf{u}(\mathbf{x})$ and the linear and angular velocities \mathbf{U}_α and $\mathbf{\Omega}_\alpha$ of the spheres can then be obtained by solving the Stokes equations for the fluid motion,

$$-\mu \nabla^2 \mathbf{u} + \nabla p = \mathbf{0}, \quad \nabla \cdot \mathbf{u} = 0, \quad (11)$$

subject to the boundary conditions

$$\mathbf{u}(\mathbf{x}) = \mathbf{u}_s(\mathbf{x}) + \mathbf{U}_\alpha + \mathbf{\Omega}_\alpha \times (\mathbf{x} - \mathbf{x}_\alpha^c), \quad \mathbf{x} \in S_\alpha, \quad (12)$$

$$\mathbf{u}(\mathbf{x}) \rightarrow \mathbf{0}, \quad |\mathbf{x}| \rightarrow \infty.$$

The formulation is closed by specifying the force and torque balance on each sphere,

$$\int_{S_\alpha} (\boldsymbol{\Sigma}^h \cdot \mathbf{n}_\alpha) dS_\alpha + \mathbf{F}_\alpha = \mathbf{0}, \quad (13)$$

$$\int_{S_\alpha} (\mathbf{x} - \mathbf{x}_\alpha^c) \times (\boldsymbol{\Sigma}^h \cdot \mathbf{n}_\alpha) dS_\alpha = \mathbf{0}, \quad (14)$$

where $\boldsymbol{\Sigma}^h = -p\mathbf{I} + \mu[\nabla\mathbf{u} + (\nabla\mathbf{u})^T]$ is the hydrodynamic stress tensor in the fluid. Note that even though DEP and ICEP occur concurrently, the linearity of the Stokes equations allows us to solve for both types of motion independently, as will be done in Sec. III.

DEP and ICEP are nonlinear phenomena that scale quadratically with the applied field \mathbf{E}_0 : reversal of the field therefore does not impact the motion, and alternating fields result in a steady motion. Making use of symmetries, it is then clear that the total external force and mean translational motion must be zero, $\mathbf{F}_1 = -\mathbf{F}_2$ and $\mathbf{U}_1 = -\mathbf{U}_2$, and the rotational motion of the two spheres must be the same, $\mathbf{\Omega}_1 = \mathbf{\Omega}_2 = \mathbf{\Omega}$. In Sec. III, we focus on determining the DEP force $\mathbf{F} = \mathbf{F}_1$ on the first sphere, and the relative velocity $\mathbf{U} = \mathbf{U}_2 - \mathbf{U}_1$ between the two spheres, along with the angular velocity $\mathbf{\Omega}$. The dependence of \mathbf{F} , \mathbf{U} , and $\mathbf{\Omega}$ on the applied field and separation vector \mathbf{R} can be written in tensorial form as

$$\mathbf{F} = 4\pi\epsilon a^2 \mathbf{F}(\lambda, \hat{\mathbf{R}}) : \mathbf{E}_0 \mathbf{E}_0, \quad (15)$$

$$\mathbf{U} = (\epsilon a / \mu) \mathbf{M}(\lambda, \hat{\mathbf{R}}) : \mathbf{E}_0 \mathbf{E}_0, \quad (16)$$

$$\mathbf{\Omega} = (\epsilon / \mu) \mathbf{W}(\lambda, \hat{\mathbf{R}}) : \mathbf{E}_0 \mathbf{E}_0, \quad (17)$$

where we have defined $\lambda = 2a/R$ and $\hat{\mathbf{R}} = \mathbf{R}/R$. \mathbf{F} and \mathbf{M} are dimensionless third-order tensors and \mathbf{W} is a dimensionless third-order pseudotensor. Using symmetries, the most gen-

eral form for these tensors can be shown to be, in indicial notation,

$$F_{ijk}(\lambda, \hat{\mathbf{R}}) = f(\lambda)(\delta_{ij}\hat{R}_k + \delta_{ik}\hat{R}_j) + g(\lambda)\hat{R}_i\delta_{jk} + h(\lambda)\hat{R}_i\hat{R}_j\hat{R}_k, \quad (18)$$

$$M_{ijk}(\lambda, \hat{\mathbf{R}}) = l(\lambda)(\delta_{ij}\hat{R}_k + \delta_{ik}\hat{R}_j) + m(\lambda)\hat{R}_i\delta_{jk} + n(\lambda)\hat{R}_i\hat{R}_j\hat{R}_k, \quad (19)$$

$$W_{ijk}(\lambda, \hat{\mathbf{R}}) = w(\lambda)\epsilon_{ijl}\hat{R}_l\hat{R}_k, \quad (20)$$

where ϵ_{ijl} is the alternating tensor, and f , g , h , l , m , n , and w are seven dimensionless scalar functions of $\lambda \in [0, 1]$. In particular, the relative motion of the two spheres is entirely determined by the four functions l , m , n , and w , the calculation of which is described next.

III. BOUNDARY-ELEMENT CALCULATIONS

A. Electric problem

We solve Laplace's equation (3) around both spheres using the boundary integral equation in its double-layer formulation (e.g., Zinchenko³²). For $\mathbf{y} \in S_\alpha$,

$$\phi(\mathbf{y}) = 2\phi_0(\mathbf{y}) + \frac{1}{2\pi} \sum_{\beta=1}^2 \int_{S_\beta} \phi(\mathbf{x}) \mathbf{n}(\mathbf{x}) \cdot \nabla G(\mathbf{y}; \mathbf{x}) dS_\mathbf{x}, \quad (21)$$

where $\phi_0(\mathbf{y}) = -\mathbf{E}_0 \cdot \mathbf{y}$ is the undisturbed external electric potential and $G(\mathbf{y}; \mathbf{x})$ is the Green's function for Laplace's equation in an infinite domain,

$$G(\mathbf{y}; \mathbf{x}) = \frac{1}{|\mathbf{y} - \mathbf{x}|}. \quad (22)$$

Note that Eq. (21) satisfies the no-flux boundary condition (4) by construction. When $\beta = \alpha$, the integral on the right-hand side of Eq. (21) is singular. This problem can be remedied using the following integral identity:

$$\int_{S_\alpha} \phi(\mathbf{x}) \mathbf{n}(\mathbf{x}) \cdot \nabla G(\mathbf{y}; \mathbf{x}) dS_\mathbf{x} = \int_{S_\alpha} [\phi(\mathbf{x}) - \phi(\mathbf{y})] \mathbf{n}(\mathbf{x}) \cdot \nabla G(\mathbf{y}; \mathbf{x}) dS_\mathbf{x} - \phi(\mathbf{y}). \quad (23)$$

The boundary integral equation (21) then becomes, for $\mathbf{y} \in S_\alpha$,

$$\phi(\mathbf{y}) - \phi_0(\mathbf{y}) = \frac{1}{4\pi} \int_{S_\alpha} [\phi(\mathbf{x}) - \phi(\mathbf{y})] \mathbf{n}(\mathbf{x}) \cdot \nabla G(\mathbf{y}; \mathbf{x}) dS_\mathbf{x} + \frac{1}{4\pi} \int_{S_{3-\alpha}} \phi(\mathbf{x}) \mathbf{n}(\mathbf{x}) \cdot \nabla G(\mathbf{y}; \mathbf{x}) dS_\mathbf{x}, \quad (24)$$

where both integrals are now regular.

Equation (24) can be solved numerically using a boundary-element method. The surface of each sphere is discretized into an unstructured highly uniform grid of six-point curved triangular elements using the algorithm of

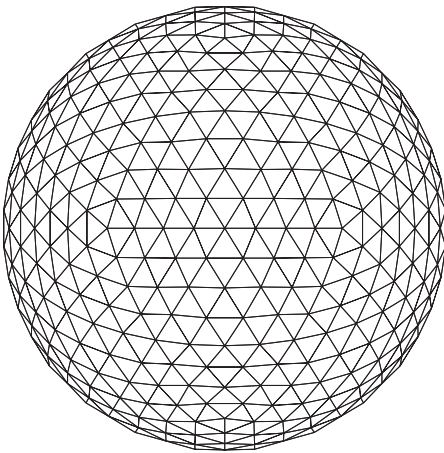


FIG. 2. Typical unstructured mesh used in the boundary-element calculations of Sec. III. The mesh was obtained using the algorithm of Loewenberg and Hinch (Ref. 33) and is composed of 1280 six-point curved triangular elements, corresponding to 3842 quadrature points.

Loewenberg and Hinch,³³ and all variables are approximated with quadratic functions over each element in terms of local triangle curvilinear coordinates (ξ, η) . This ensures second-order accuracy for the evaluation of the integrals.³⁴ Figure 2 shows a typical mesh used in the calculations, with 1280 triangles corresponding to 3842 quadrature points.

Once the value of the potential ϕ has been obtained on the surface of the spheres, the surface electric field is calculated as $\mathbf{E}(\mathbf{x}) = -\nabla_s \phi(\mathbf{x})$, where the surface gradient $\nabla_s \phi = (\mathbf{I} - \mathbf{nn}) \cdot \nabla \phi$ is determined by solving a 3×3 linear system at each quadrature point on the spheres (e.g., Pozrikidis³⁵),

$$\frac{\partial \mathbf{x}}{\partial \xi} \cdot \nabla_s \phi = \frac{\partial \phi}{\partial \xi}, \quad \frac{\partial \mathbf{x}}{\partial \eta} \cdot \nabla_s \phi = \frac{\partial \phi}{\partial \eta}, \quad \mathbf{n} \cdot \nabla_s \phi = 0. \quad (25)$$

Knowledge of the surface electric field then allows the determination of the Maxwell stress tensor using Eq. (2), from which the dielectrophoretic forces are calculated using Eq. (6). Results of the calculations for the functions $f(\lambda)$, $g(\lambda)$, and $h(\lambda)$ are shown in Fig. 3. They are also compared to asymptotic results obtained using the method of reflections^{28,29} and the more general method of twin multipole expansions,^{30,36} which is described in the Appendix. In particular, the asymptotic results obtained by the method of reflections are

$$f(\lambda) = -\frac{3}{64}\lambda^4 + O(\lambda^6), \quad (26)$$

$$g(\lambda) = -\frac{3}{64}\lambda^4 + O(\lambda^6), \quad (27)$$

$$h(\lambda) = \frac{15}{64}\lambda^4 + O(\lambda^6). \quad (28)$$

We find excellent agreement between the boundary-element calculations and the method of twin multipole expansions, in which 50 terms were retained in the expansions to ensure an error of less than 1% at $\lambda = 0.98$ (or $R/a \approx 2.05$). The method of reflections to $O(\lambda^6)$ [Eqs. (26)–(28)] performs well for $\lambda \leq 0.6$, i.e., $R/a \geq 3.3$, but fails to capture the correct force magnitude at shorter separation distances. From the sign of

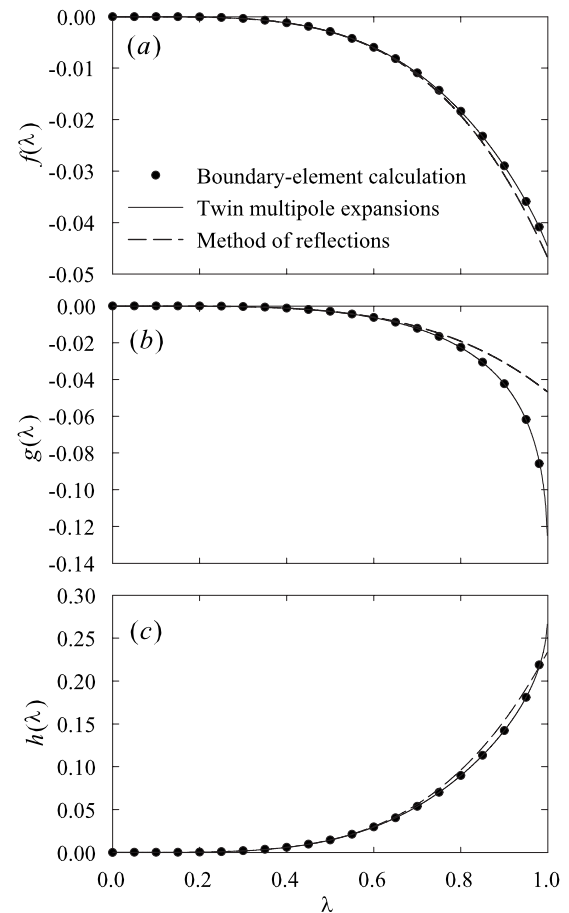


FIG. 3. Dimensionless coefficients (a) $f(\lambda)$, (b) $g(\lambda)$, and (c) $h(\lambda)$ in the general expression (18) for the DEP force \mathbf{F} as functions of $\lambda = 2a/R \in [0, 1]$. The plots show results from the boundary-element calculations of Sec. III A, from the method of twin multipole expansions (Refs. 30 and 36) (cf. the Appendix) in which 50 terms were retained in the expansions, and from the method of reflections (Refs. 28 and 29) [Eqs. (26)–(28)].

the functions $f(\lambda)$, $g(\lambda)$, and $h(\lambda)$, it can be shown that the DEP forces on the spheres are attractive when the spheres are aligned in the direction of the electric field ($\mathbf{E}_0 \cdot \hat{\mathbf{R}} = \pm E_0$), whereas they are repulsive when the spheres are aligned in a perpendicular direction ($\mathbf{E}_0 \cdot \hat{\mathbf{R}} = 0$). The precise particle motions resulting from these forces are calculated in Sec. III B.

An important result visible from Eqs. (26)–(28) is the far-field decay of the DEP force as $O(\lambda^4) = O(R^{-4})$. This decay is quite fast and significantly faster than the decay of interactions in other common particulate flows, such as sedimentation or shear flow, in which it is of $O(\lambda)$ and $O(\lambda^2)$, respectively. These DEP interactions are therefore expected to be quite weak unless the particles are very close to each other. Note that a similar $O(\lambda^4)$ dependence had been obtained by Yariv¹¹ for the decay of the DEP force on a single sphere near a planar wall.

As pointed out by Yariv,¹¹ there is a close analogy between the DEP forces calculated here and pressure forces in incompressible and inviscid potential flows. It should therefore be noted that the functions f , g , and h had previously been obtained in the context of interactions between spherical bubbles in inviscid flow,^{37,38} a problem governed by nearly identical equations.

B. Flow problem

The Stokes equations (11) around the two spheres are then solved using a deflated double-layer boundary integral equation (see Pozrikidis^{34,39} for a detailed derivation). Denoting by \mathbf{q} the double-layer potential strength, we have for $\mathbf{y} \in S_\alpha$,

$$\begin{aligned} 4\pi\mathbf{q}(\mathbf{y}) = & - \sum_{\beta=1}^2 \int_{S_\beta} \mathbf{q}(\mathbf{x}) \cdot \mathbb{T}(\mathbf{y};\mathbf{x}) \cdot \mathbf{n}(\mathbf{x}) dS_{\mathbf{x}} \\ & + \frac{\mathbf{n}(\mathbf{y})}{a^2} \int_{S_\alpha} \mathbf{n}(\mathbf{x}) \cdot \mathbf{q}(\mathbf{x}) dS_{\mathbf{x}} + \mathbf{U}_\alpha + \boldsymbol{\Omega}_\alpha \\ & \times (\mathbf{y} - \mathbf{x}_\alpha^c) - \mathbf{u}_s(\mathbf{y}) + \frac{1}{8\pi\mu} \sum_{\beta=1}^2 \mathbf{J}(\mathbf{y};\mathbf{x}_\beta^c) \cdot \mathbf{F}_\beta, \end{aligned} \quad (29)$$

where $\mathbf{J}(\mathbf{y};\mathbf{x})$ and $\mathbb{T}(\mathbf{y};\mathbf{x})$ denote the Stokeslet and stresslet Green's functions in an infinite domain, respectively,

$$\mathbf{J}(\mathbf{y};\mathbf{x}) = \frac{1}{|\mathbf{y} - \mathbf{x}|} + \frac{(\mathbf{y} - \mathbf{x})(\mathbf{y} - \mathbf{x})}{|\mathbf{y} - \mathbf{x}|^3}, \quad (30)$$

$$\mathbb{T}(\mathbf{y};\mathbf{x}) = -6 \frac{(\mathbf{y} - \mathbf{x})(\mathbf{y} - \mathbf{x})(\mathbf{y} - \mathbf{x})}{|\mathbf{y} - \mathbf{x}|^5}. \quad (31)$$

In Eq. (29), the slip velocity $\mathbf{u}_s(\mathbf{y})$ on the sphere surfaces is calculated using Eq. (7), where the nonuniform surface zeta potential and surface electric field were obtained when solving the electric problem around the spheres in Sec. III A [the zeta potential is directly related to the surface electric potential through Eq. (8)]. Finally, to complete the boundary integral formulation, we relate the linear and angular velocities \mathbf{U}_α and $\boldsymbol{\Omega}_\alpha$ of the spheres to the double-layer potential strength by

$$\mathbf{U}_\alpha = -\frac{1}{a^2} \int_{S_\alpha} \mathbf{q}(\mathbf{x}) dS_{\mathbf{x}}, \quad (32)$$

$$\boldsymbol{\Omega}_\alpha = -\frac{3}{2a^4} \int_{S_\alpha} (\mathbf{x} - \mathbf{x}_\alpha^c) \times \mathbf{q}(\mathbf{x}) dS_{\mathbf{x}}. \quad (33)$$

When $\beta = \alpha$, the first integral in Eq. (29) is singular. In a similar fashion as in Sec. III A, this singularity can be removed using the following integral identity:³⁴

$$\begin{aligned} & \int_{S_\alpha} \mathbf{q}(\mathbf{x}) \cdot \mathbb{T}(\mathbf{y};\mathbf{x}) \cdot \mathbf{n}(\mathbf{x}) dS_{\mathbf{x}} \\ & = \int_{S_\alpha} [\mathbf{q}(\mathbf{x}) - \mathbf{q}(\mathbf{y})] \cdot \mathbb{T}(\mathbf{y};\mathbf{x}) \cdot \mathbf{n}(\mathbf{x}) dS_{\mathbf{x}} - 4\pi\mathbf{q}(\mathbf{y}), \end{aligned} \quad (34)$$

where the integral on the right-hand side is now regular. Upon substitution of Eq. (34) into Eq. (29), we arrive at the following integral equation:

$$\begin{aligned} & \int_{S_\alpha} [\mathbf{q}(\mathbf{x}) - \mathbf{q}(\mathbf{y})] \cdot \mathbb{T}(\mathbf{y};\mathbf{x}) \cdot \mathbf{n}(\mathbf{x}) dS_{\mathbf{x}} \\ & + \int_{S_{3-\alpha}} \mathbf{q}(\mathbf{x}) \cdot \mathbb{T}(\mathbf{y};\mathbf{x}) \cdot \mathbf{n}(\mathbf{x}) dS_{\mathbf{x}} \\ & - \frac{\mathbf{n}(\mathbf{y})}{a^2} \int_{S_\alpha} \mathbf{n}(\mathbf{x}) \cdot \mathbf{q}(\mathbf{x}) dS_{\mathbf{x}} - \mathbf{U}_\alpha - \boldsymbol{\Omega}_\alpha \times (\mathbf{y} - \mathbf{x}_\alpha^c) \\ & = -\mathbf{u}_s(\mathbf{y}) + \frac{1}{8\pi\mu} \sum_{\beta=1}^2 \mathbf{J}(\mathbf{y};\mathbf{x}_\beta^c) \cdot \mathbf{F}_\beta, \end{aligned} \quad (35)$$

where \mathbf{U}_α and $\boldsymbol{\Omega}_\alpha$ are still expressed by Eqs. (32) and (33). Equation (35) was solved numerically using a similar boundary-element method as in Sec. III A for the electric potential, on an unstructured grid of six-point curved triangular elements. Because of the higher dimensionality of the double-layer potential in the flow problem, a slightly coarser mesh was typically used than for the solution of the electric potential, resulting in slightly larger discretization errors at short separation distances.

It should be noted that the forcing terms in Eq. (35) have two origins: the DEP forces \mathbf{F}_β on the spheres and the slip velocity \mathbf{u}_s will both result in fluid and particle motions. Because Eq. (35) is linear with respect to the double-layer potential and to velocities (a direct consequence of the linearity of the Stokes equations), these two types of motions can be solved separately and superimposed.

Equation (35) was first solved for the DEP motions by setting the slip velocity to zero, and results for the functions $l^{\text{DEP}}(\lambda)$, $m^{\text{DEP}}(\lambda)$, $n^{\text{DEP}}(\lambda)$, and $w^{\text{DEP}}(\lambda)$ corresponding to the DEP motion alone are plotted in Fig. 4. As in the case of the DEP force (Fig. 3), we compare the results of the boundary element calculations to results obtained by the method of twin multipole expansions (with 20 terms in the expansions) and to the following asymptotic results from the method of reflections:

$$l^{\text{DEP}}(\lambda) = \frac{1}{16}\lambda^4 - \frac{3}{128}\lambda^5 + O(\lambda^6), \quad (36)$$

$$m^{\text{DEP}}(\lambda) = \frac{1}{16}\lambda^4 - \frac{3}{64}\lambda^5 + O(\lambda^6), \quad (37)$$

$$n^{\text{DEP}}(\lambda) = -\frac{5}{16}\lambda^4 + \frac{3}{16}\lambda^5 + O(\lambda^6), \quad (38)$$

$$w^{\text{DEP}}(\lambda) = \frac{3}{512}\lambda^6 + O(\lambda^7). \quad (39)$$

Once again, we find that excellent agreement is obtained between the boundary element calculations and the method of twin multipole expansions (except at very short separation distances, which is a consequence of the coarser mesh used in the boundary-element discretization) and that the method of reflections performs adequately for $\lambda \lesssim 0.6$.

Similarly, results were obtained for the ICEP motion by retaining the slip velocity in Eq. (35) but setting the DEP forces to zero. They are plotted in Fig. 5 against the twin multipole expansion results and the following asymptotic expansions from the method of reflections:

$$l^{\text{ICEP}}(\lambda) = -\frac{11}{32}\lambda^4 + O(\lambda^6), \quad (40)$$

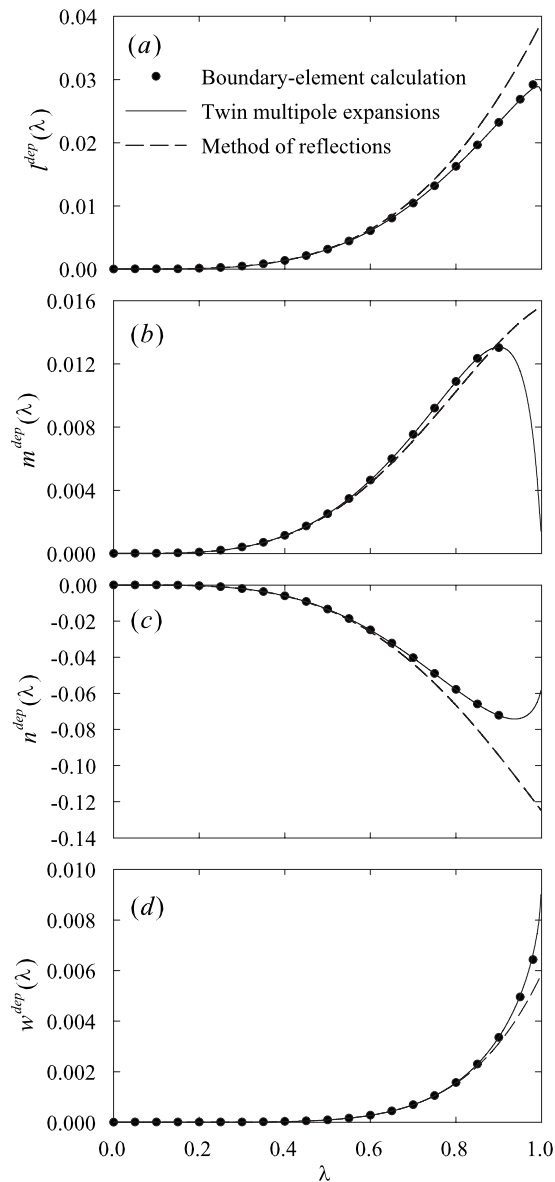


FIG. 4. Dimensionless coefficients (a) $l^{\text{DEP}}(\lambda)$, (b) $m^{\text{DEP}}(\lambda)$, (c) $n^{\text{DEP}}(\lambda)$, and (d) $w^{\text{DEP}}(\lambda)$ in the general expressions (19) and (20) for the DEP linear and angular velocities \mathbf{U}^{DEP} and $\mathbf{\Omega}^{\text{DEP}}$ as functions of $\lambda=2a/R \in [0, 1]$. The plots show results from the boundary-element calculations of Sec. III B, from the method of twin multipole expansions³¹ (cf. the Appendix), in which 20 terms were retained in the expansions, and from the method of reflections [Refs. 28 and 29] [Eqs. (36)–(39)].

$$m^{\text{ICEP}}(\lambda) = \frac{9}{16}\lambda^2 - \frac{11}{32}\lambda^4 + \frac{27}{64}\lambda^5 + O(\lambda^6), \quad (41)$$

$$n^{\text{ICEP}}(\lambda) = -\frac{27}{16}\lambda^2 + \frac{55}{32}\lambda^4 - \frac{27}{32}\lambda^5 + O(\lambda^6), \quad (42)$$

$$w^{\text{ICEP}}(\lambda) = \frac{27}{64}\lambda^3 + O(\lambda^6). \quad (43)$$

These results should be compared to the previous derivations of Dukhin and co-workers,^{14–16} in which only the leading-order terms to $O(\lambda^4)$ had been obtained. An important point to be made here is the $O(\lambda^2)$ decay of the ICEP relative velocity, as seen in Eqs. (41) and (42). This dependence is a direct consequence of the leading-order stresslet flow generated by a single sphere undergoing ICEP (Ref. 19) and is significantly slower than the $O(\lambda^4)$ decay of the interactions

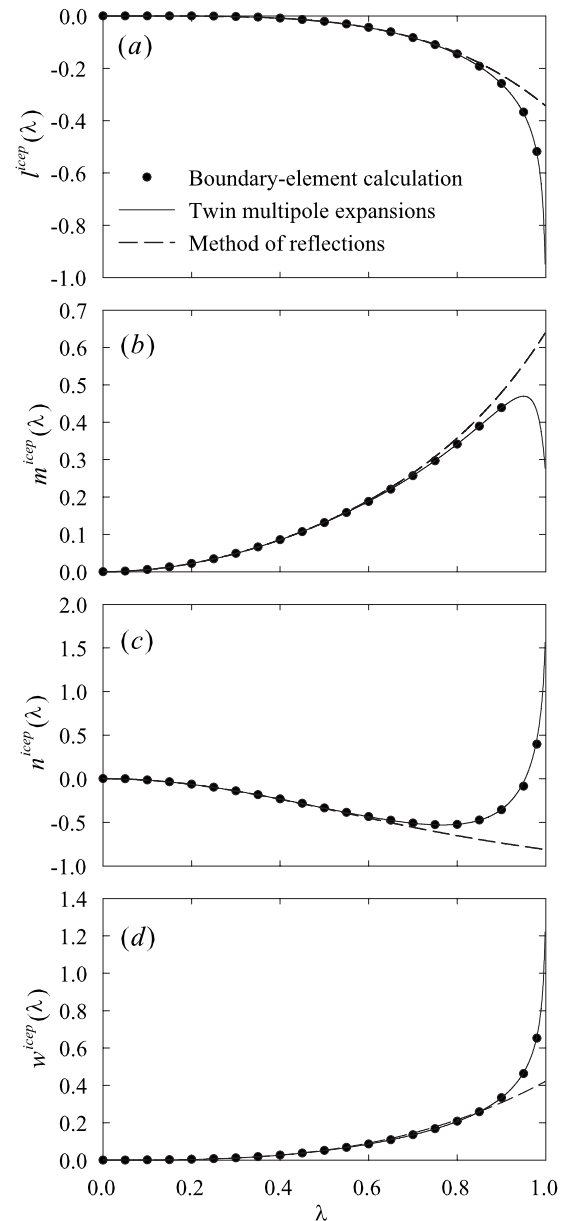


FIG. 5. Dimensionless coefficients (a) $l^{\text{ICEP}}(\lambda)$, (b) $m^{\text{ICEP}}(\lambda)$, (c) $n^{\text{ICEP}}(\lambda)$, and (d) $w^{\text{ICEP}}(\lambda)$ in the general expressions (19) and (20) for the ICEP linear and angular velocities \mathbf{U}^{ICEP} and $\mathbf{\Omega}^{\text{ICEP}}$ as functions of $\lambda=2a/R \in [0, 1]$. The plots show results from the boundary-element calculations of Sec. III B, from the method of twin multipole expansions (Ref. 31) (cf. the Appendix), in which 20 terms were retained in the expansions, and from the method of reflections (Refs. 28 and 29) [Eqs. (40)–(43)].

from DEP, as found in Fig. 4 and Eqs. (36)–(39). We can therefore expect ICEP to dominate the motion when particle polarizability is significant.

Finally, results for the total relative motion including both DEP and ICEP were obtained by superimposing the results of Figs. 4 and 5 and are shown in Fig. 6. In this case, the asymptotic expansions for the various coefficients obtained by the method of reflections are given by

$$l(\lambda) = -\frac{9}{32}\lambda^4 - \frac{3}{128}\lambda^5 + O(\lambda^6), \quad (44)$$

$$m(\lambda) = \frac{9}{16}\lambda^2 - \frac{9}{32}\lambda^4 + \frac{3}{8}\lambda^5 + O(\lambda^6), \quad (45)$$

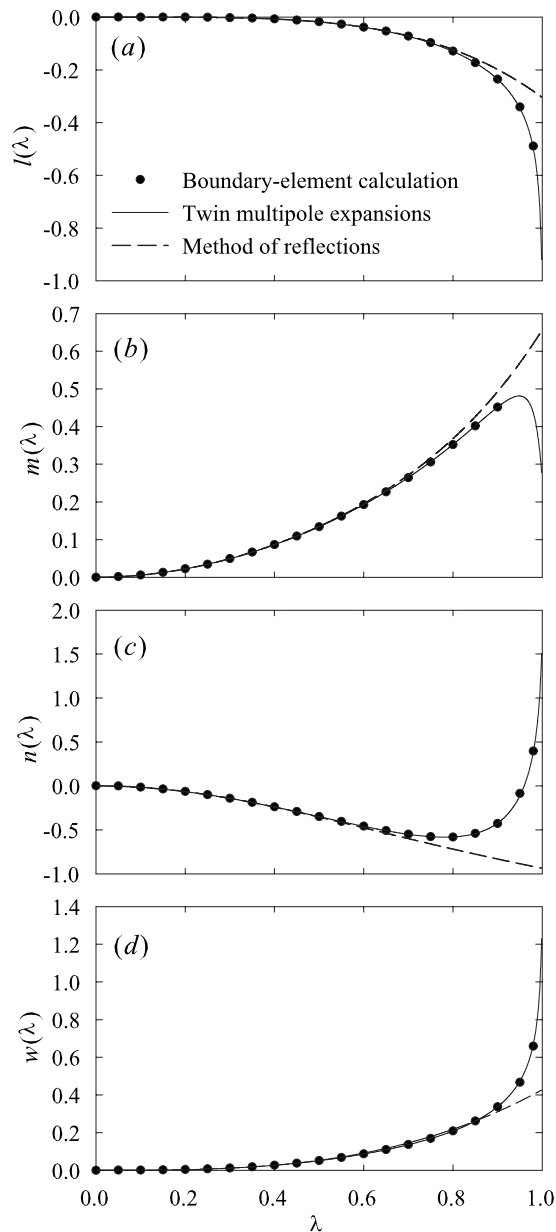


FIG. 6. Dimensionless coefficients (a) $l(\lambda)$, (b) $m(\lambda)$, (c) $n(\lambda)$, and (d) $w(\lambda)$ in the general expressions (19) and (20) for the total linear and angular velocities \mathbf{U} and $\mathbf{\Omega}$ (including both DEP and ICEP) as functions of $\lambda = 2a/R \in [0, 1]$. The plots show results from the boundary-element calculations of Sec. III B, from the method of twin multipole expansions (Ref. 31) (cf. the Appendix), in which 20 terms were retained in the expansions, and from the method of reflections (Refs. 28 and 29) [Eqs. (44)–(47)].

$$n(\lambda) = -\frac{27}{16}\lambda^2 + \frac{45}{32}\lambda^4 - \frac{21}{32}\lambda^5 + O(\lambda^6), \quad (46)$$

$$w(\lambda) = \frac{27}{64}\lambda^3 + O(\lambda^6). \quad (47)$$

A quick comparison of Figs. 5 and 6 clearly shows that the motion is strongly dominated by ICEP, due to the stronger $O(\lambda^2)$ dependence of the ICEP relative velocity. Note that while the $O(\lambda^2)$ decay of the ICEP velocity is a general result, the magnitude of that velocity would be expected to be weaker if the particles were not ideally polarizable

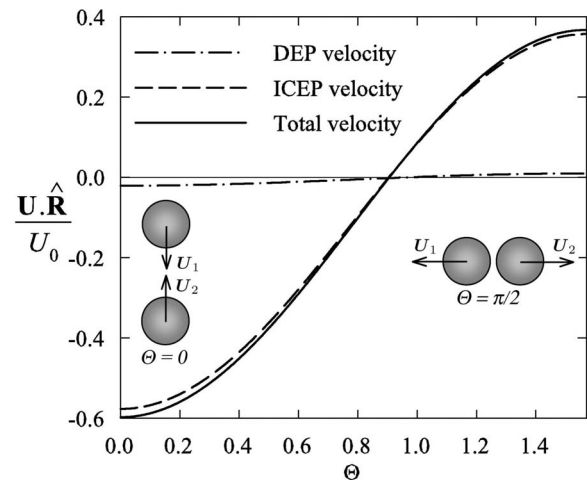


FIG. 7. Radial component $\mathbf{U} \cdot \hat{\mathbf{R}}$ of the relative velocity between the two spheres scaled by the velocity scale $U_0 = (\epsilon a / \mu) E_0^2$ as a function of the angle Θ made between the external field and the line of centers of the two spheres ($\mathbf{E}_0 \cdot \hat{\mathbf{R}} = E_0 \cos \Theta$). The radial velocity was calculated using Eq. (48) for $\lambda = 0.8$ (or, equivalently, $R/a = 2.5$). The plot shows the velocities arising from DEP and ICEP, as well as the total velocity when both effects are present.

(for example, if they were dielectrics). There could therefore be circumstances under which DEP dominates ICEP at short separation distances.

IV. TRAJECTORIES AND FAR-FIELD FLOW DISTURBANCE

We now discuss the nature of the motions that result from these interactions. Figure 7 shows the radial component of the relative velocity $\mathbf{U} \cdot \hat{\mathbf{R}}$ between the two spheres as a function of the angle Θ made between the direction of the external field and the line of center between the two spheres: $\mathbf{E}_0 \cdot \hat{\mathbf{R}} = E_0 \cos \Theta$. This radial velocity is easily evaluated by means of Eqs. (16) and (19) as

$$\frac{\mathbf{U} \cdot \hat{\mathbf{R}}}{U_0} = [2l(\lambda) + n(\lambda)] \cos^2 \Theta + m(\lambda), \quad (48)$$

where $U_0 = (\epsilon a / \mu) E_0^2$ is the velocity scale for the DEP and ICEP motions. In agreement with our observations of Sec. III B, the ICEP motion is found to strongly dominate the particle motions at the intermediate separation distance of $R/a = 2.5$, at which the results of Fig. 7 were calculated; both motions, however, almost always have the same direction radially (expect in a very small region near the angle at which $\mathbf{U} \cdot \hat{\mathbf{R}}$ switches sign). In particular, the relative radial velocity is negative for low values of Θ , which corresponds to particle attraction, but becomes positive for $\Theta \geq 0.9$ rad (or 51.5°), beyond which the particles are repelled. The attraction and the repulsion are the strongest when the particles are aligned with or perpendicular to the direction of the external field, respectively ($\Theta = 0$ and $\Theta = \pi/2$).

The pair dynamics resulting from these interactions are easy to anticipate: particles will attract along the direction of the electric field, pair up, and separate in the transverse direction. This is illustrated in Fig. 8, showing a typical trajec-

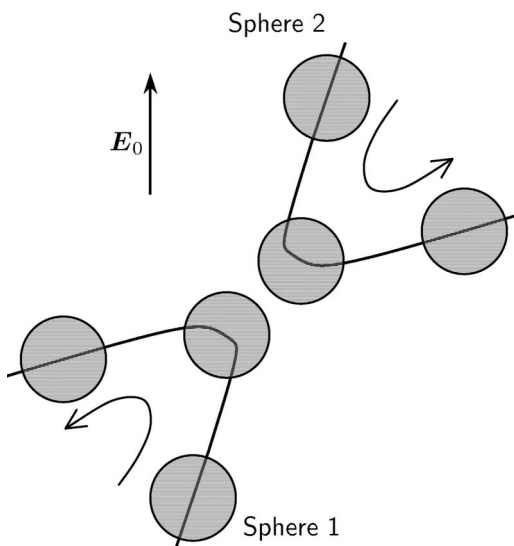


FIG. 8. Typical trajectories of two spheres undergoing DEP and ICEP in an electric field \mathbf{E}_0 . The two spheres are attracted in the direction of the field, pair up, and then separate in the transverse direction. The arrows indicate the direction of motion.

tory for the motion of the two spheres. This trajectory is qualitatively very similar to those obtained previously in the case of rodlike particles²² (note, however, that for high-aspect ratio rods, DEP interactions are significantly weaker than for spheres as they scale with the rod thickness²² and can be safely neglected with respect to ICEP). When particles meet head on (or nearly head on) in the direction of the field, long-lasting pairing may be expected and may possibly result in chaining in suspensions of many particles. In addition, we can also expect that an initially spherical cloud of such particles placed in an electric field will compress in the direction of the field and stretch in the perpendicular directions as a result of these interactions.

We finish by commenting on the far-field decay of the fluid velocity away from a pair of spheres subject to DEP and ICEP. Denote by \mathbf{x} a position vector emanating from the center point between the two spheres. For two nonpolarizable spheres with fixed and uniform zeta potential ζ undergoing standard electrophoresis, the leading-order term in an expansion of the fluid velocity far away from the spheres (i.e., when $R \ll |\mathbf{x}|$) can be shown to be

$$\mathbf{u}^{\text{EP}}(\mathbf{x}) \approx \frac{\varepsilon \zeta}{\mu} \left(\frac{a}{r} \right)^3 (3\hat{\mathbf{x}}\hat{\mathbf{x}} - \mathbf{1}) \cdot \mathbf{E}_0, \quad (49)$$

where $r = |\mathbf{x}|$ and $\hat{\mathbf{x}} = \mathbf{x}/r$. This electrophoretic disturbance flow is a potential flow (not only in the far field) and decays fairly rapidly like r^{-3} away from the two spheres. The far-field disturbance flows induced by DEP and ICEP are, however, qualitatively different, as they are no longer potential and have a slower far-field decay. Their leading-order terms can be shown to be

$$\begin{aligned} \mathbf{u}^{\text{DEP}}(\mathbf{x}) \approx & \frac{1}{2} \frac{\varepsilon R}{\mu} \left(\frac{a}{r} \right)^2 [\hat{\mathbf{x}}\hat{\mathbf{R}} + \hat{\mathbf{R}}\hat{\mathbf{x}} - (\hat{\mathbf{x}} \cdot \hat{\mathbf{R}}) \\ & \times (\mathbf{1} + 3\hat{\mathbf{x}}\hat{\mathbf{x}})] \cdot \mathbf{F}(\lambda, \hat{\mathbf{R}}) \cdot \mathbf{E}_0 \mathbf{E}_0, \end{aligned} \quad (50)$$

$$\mathbf{u}^{\text{ICEP}}(\mathbf{x}) \approx \frac{9}{4} \frac{\varepsilon a}{\mu} \left(\frac{a}{r} \right)^2 \hat{\mathbf{x}} (\mathbf{1} - 3\hat{\mathbf{x}}\hat{\mathbf{x}}) \cdot \mathbf{E}_0 \mathbf{E}_0, \quad (51)$$

where $\mathbf{F}(\lambda, \hat{\mathbf{R}})$ is given by Eq. (18). Unlike $\mathbf{u}^{\text{EP}}(\mathbf{x})$, these two flows are now rotational. They are both Stokes dipole flows in the far field and decay slowly like r^{-2} . Note that because $\mathbf{F}(\lambda, \hat{\mathbf{R}}) = O(\lambda^4)$, in general, we can expect to have $|\mathbf{u}^{\text{DEP}}(\mathbf{x})| \ll |\mathbf{u}^{\text{ICEP}}(\mathbf{x})|$, i.e., the fluid flow will be dominated by ICEP.

V. CONCLUDING REMARKS

We have shown that particles undergoing electrophoresis in a viscous electrolyte may also be subject to two other types of nonlinear electrokinetic effects.⁴⁰ The first effect, termed DEP by analogy to the motion of a single particle in a nonuniform electric field,¹¹ is a consequence of the distortion of the external electric field when several particles are present in suspension and results in nonzero electric forces scaling quadratically with the applied field. In particular, these forces should arise even for nonpolarizable particles. The second effect, termed ICEP,¹⁹ occurs when the particles are able to polarize and results from the flows driven inside the nonuniform charge clouds that form around the particle surfaces. These effects (and, in particular, DEP) may have been overlooked in the past in studies of electrophoresis on the basis that they scale quadratically with the applied field and should therefore be negligible in weak fields. However, a simple scaling argument shows otherwise.¹¹ While the scale for the classical electrophoretic velocity of a single particle is $O(\varepsilon \zeta E_0 / \mu)$, the scale for the DEP and ICEP relative velocities is $O(\varepsilon a E_0^2 / \mu)$; the latter will therefore become significant when $a E_0 / \zeta = O(1)$, which may occur for moderate particle sizes or moderate field strengths, as well as for particles with very low native zeta potentials.

As we have shown, both DEP and ICEP result in relative motions, and the relative velocities between a pair of identical ideally polarizable spheres were calculated with good accuracy for a wide range of separation distances, using three different methods. In particular, we found that both DEP and ICEP cause the particles to be attracted when they are aligned with the external field and repelled when they are aligned in a perpendicular direction. This results in pairing dynamics by which particles attract along the direction of the field, pair up, and separate in the transverse direction. Even though both DEP and ICEP contribute to these motions, ICEP was found to strongly dominate the motion in the case of ideally polarizable particles, due to its slower decay with separation distance as $O(R^{-2})$ vs $O(R^{-4})$ for DEP interactions. Another interesting consequence of these effects is the qualitatively different nature of the disturbance flow field away from a pair of particles, which is no longer potential as in the case of classical electrophoresis and decays more slowly like $O(r^{-2})$ with the distance r from the location of the sphere pair.

While our calculations have provided accurate results for the particle motions down to very short separation distances (with errors of less than 1% at $R/a = 2.05$ with the method of twin multipole expansions), they are all based on far-field

descriptions of the hydrodynamics and cannot capture precisely the dynamics when the particles are almost at contact. In this case, a lubrication theory could be developed to complement the results presented in this work, in the spirit of the analysis of Yariv and Brenner⁴² for classical electrophoresis. Note, however, that the coupling between the electric and flow problems for DEP and ICEP is more complex than for standard electrophoresis and would make any lubrication analysis significantly more involved. In addition, we can expect the thin-double-layer assumption used here to break down when the separation distance between the sphere surfaces becomes of the order of the Debye length (or thickness of the screening layer): in this case, a different analysis accounting for diffuse charge dynamics around the particles would be required. While such an analysis was recently proposed by Yariv and Miloh⁴³ to describe ICEP around a single sphere, it has yet to be attempted to model interactions between particles.

APPENDIX: METHOD OF TWIN MULTIPOLE EXPANSIONS

The method of twin multipole expansions is a systematic generalization of the method of reflections^{28,29} and was described by Jeffrey³⁰ in the case of Laplace interactions and by Jeffrey and Onishi³¹ in the case of Stokes interactions. For Laplace interactions, it consists in seeking the electric potential in the vicinity of sphere α as an expansion in growing and decaying spherical harmonics,

$$\phi^{(\alpha)}(\mathbf{x}) = \phi_0(\mathbf{x}) + \sum_{n=0}^{\infty} \sum_{m=0}^1 \left[\tilde{\Phi}_{nm}^{\alpha} \left(\frac{r_{\alpha}}{a} \right)^{-n-1} + \hat{\Phi}_{nm}^{\alpha} \left(\frac{r_{\alpha}}{a} \right)^n \right] P_n^m(\cos \theta_{\alpha}) \cos m\psi, \quad (\text{A1})$$

where r_{α} is the distance from position \mathbf{x} to the center of sphere α and the angles θ_{α} and ψ are defined in Fig. 1. P_n^m denote the associated Legendre polynomials⁴⁴ and $\tilde{\Phi}_{nm}^{\alpha}$ and $\hat{\Phi}_{nm}^{\alpha}$ are unknown constant coefficients to be determined. To obtain these coefficients, we require that the two expansions $\phi^{(1)}$ and $\phi^{(2)}$ match far away from either sphere, which can be shown to yield the following condition:³⁰

$$\hat{\Phi}_{nm}^{(\alpha)} = \left(\frac{a}{R} \right)^n \sum_{l=m}^{\infty} \binom{l+n}{n+m} \left(\frac{a}{R} \right)^{l+1} \tilde{\Phi}_{lm}^{(3-\alpha)}. \quad (\text{A2})$$

In addition, we need to make sure that the no-flux boundary condition $\mathbf{n}_{\alpha} \cdot \nabla \phi^{(\alpha)}(\mathbf{x}) = 0$ is enforced on the surface of sphere α . Noting that $\mathbf{n}_{\alpha} \cdot \nabla \phi_0^{(\alpha)}(\mathbf{x}) = -\mathbf{n}_{\alpha} \cdot \mathbf{E}_0$ can be expanded on the basis of surface harmonics as follows:

$$\mathbf{n}_{\alpha} \cdot \nabla \phi_0^{(\alpha)}(\mathbf{x}) = -E_{\parallel} P_1^0(\cos \theta_{\alpha}) + (-1)^{\alpha-1} \times E_{\perp} P_1^1(\cos \theta_{\alpha}) \cos \psi, \quad (\text{A3})$$

where E_{\parallel} and E_{\perp} are the components of the applied field \mathbf{E}_0 in the directions parallel and perpendicular to the line of centers, respectively, and using the orthogonality property

of spherical harmonics, it can be shown that the no-flux boundary condition on the surface of sphere α is equivalent to

$$aE_{\parallel} \delta_{n1} \delta_{m0} + (-1)^{\alpha} aE_{\perp} \delta_{n1} \delta_{m1} - (n+1) \hat{\Phi}_{nm}^{\alpha} + n \tilde{\Phi}_{nm}^{\alpha} = 0, \quad (\text{A4})$$

where δ_{ij} denotes the Kronecker delta. Equations (A2) and (A4) constitute a linear system for the expansion coefficients $\tilde{\Phi}_{nm}^{\alpha}$ and $\hat{\Phi}_{nm}^{\alpha}$, which can be inverted numerically after truncation of the sum in Eq. (A2). For the calculations shown on Fig. 3, 50 terms were retained in the sum.

After the coefficients $\tilde{\Phi}_{nm}^{\alpha}$ and $\hat{\Phi}_{nm}^{\alpha}$ for the electric potential have been obtained, the dielectrophoretic forces on the spheres can be calculated directly using a method proposed by Washizu,³⁶ to which the reader is referred for details. Washizu³⁶ also explained how the coefficients can be used to obtain an expansion for the electric field. Once the electric field and potential are known on the sphere surfaces, they can be multiplied to yield the slip velocity $\mathbf{u}_s(\mathbf{x})$ [Eq. (7)], which itself can then be re-expanded on the basis of surface harmonics.

A similar method, also based on twin multipole expansions, can then be applied to determine the fluid and particle motions. The method was described in detail by Jeffrey and Onishi³¹ for the determination of the mobility of a pair of rigid spheres, and for brevity is not repeated here. It consists again in representing the flow variables (fluid velocity and pressure) using Lamb's general solution for Stokes flow²⁸ as a sum of two expansions in decaying harmonics emanating from both sphere centers. Scalar equations for the coefficients in the expansions are then obtained by application of a matching condition and of the boundary condition [Eq. (12)], where the slip velocity was obtained as described above from Eq. (7) and from the expansions for the surface electric field and potential. Together with force and torque balances on the spheres, these equations constitute a closed linear system for the velocity and pressure expansion coefficients, which is inverted after truncation of the sums. This allows the determination of the particle linear and angular velocities (Figs. 4–6).

¹D. A. Saville, "Electrokinetic effects with small particles," *Annu. Rev. Fluid Mech.* **9**, 321 (1977).

²J. L. Anderson, "Colloid transport by interfacial forces," *Annu. Rev. Fluid Mech.* **21**, 61 (1989).

³W. B. Russel, D. A. Saville, and W. R. Schowalter, *Colloidal Dispersions* (Cambridge University Press, Cambridge, 1989).

⁴T. B. Jones, *Electromechanics of Particles* (Cambridge University Press, Cambridge, 1995).

⁵A. Ramos, H. Morgan, N. G. Green, and A. Castellanos, "AC electrokinetics: A review of forces in microelectrode structures," *J. Phys. D* **31**, 2338 (1998).

⁶N. G. Green and H. Morgan, "Separation of submicrometer particles using a combination of dielectrophoretic and electrohydrodynamic forces," *J. Phys. D* **31**, 25 (1998).

⁷L. D. Reed and F. A. Morrison, "Hydrodynamic interaction in electrophoresis," *J. Colloid Interface Sci.* **54**, 117 (1976).

⁸A. Acrivos, D. J. Jeffrey, and D. A. Saville, "Particle migration in suspensions by thermocapillary or electrophoretic motion," *J. Fluid Mech.* **212**, 95 (1990).

⁹J. L. Viovy, "Electrophoresis of DNA and other polyelectrolytes: Physical mechanisms," *Rev. Mod. Phys.* **72**, 813 (2000).

- ¹⁰T. S. Simonova, V. N. Shilov, and O. A. Shramko, "Low-frequency dielectrophoresis and the polarization interaction of uncharged spherical particles with an induced Debye atmosphere of arbitrary thickness," *Colloid J.* **63**, 114 (2001).
- ¹¹E. Yariv, "Force-free electrophoresis?," *Phys. Fluids* **18**, 031702 (2006).
- ¹²V. G. Levich, *Physicochemical Hydrodynamics* (Prentice-Hall, Englewood Cliffs, NJ, 1962).
- ¹³I. N. Simonov and A. S. Dukhin, "Theory of electrophoresis of solid conducting particles in case of ideal polarization of a thin diffuse double layer," *Colloid J.* **35**, 173 (1973).
- ¹⁴N. I. Gamayunov, V. A. Murtsovkin, and A. S. Dukhin, "Pair interaction of particles in electric field. 1. Features of hydrodynamic interaction of polarized particles," *Colloid J. USSR* **48**, 197 (1986).
- ¹⁵A. S. Dukhin and V. A. Murtsovkin, "Pair interaction of particles in electric field. 2. Influence of polarization of double layer of dielectric particles on their hydrodynamic interaction in a stationary electric field," *Colloid J. USSR* **48**, 203 (1986).
- ¹⁶A. S. Dukhin, "Pair interaction of particles in electric field. 3. Hydrodynamic interaction of ideally polarizable metal particles and dead biological cells," *Colloid J. USSR* **48**, 376 (1986).
- ¹⁷V. A. Murtsovkin, "Nonlinear flows near polarized dispersed particles," *Colloid J.* **58**, 341 (1996).
- ¹⁸M. Z. Bazant and T. M. Squires, "Induced-charge electrokinetic phenomena: Theory and microfluidic applications," *Phys. Rev. Lett.* **92**, 066101 (2004).
- ¹⁹T. M. Squires and M. Z. Bazant, "Induced-charge electro-osmosis," *J. Fluid Mech.* **509**, 217 (2004).
- ²⁰T. M. Squires and M. Z. Bazant, "Breaking symmetries in induced-charge electro-osmosis and electrophoresis," *J. Fluid Mech.* **560**, 65 (2006).
- ²¹E. Yariv, "Induced-charge electrophoresis of non-spherical particles," *Phys. Fluids* **17**, 051702 (2005).
- ²²D. Saintillan, E. Darve, and E. S. G. Shaqfeh, "Hydrodynamic interactions in the induced-charge electrophoresis of colloidal rod dispersions," *J. Fluid Mech.* **563**, 223 (2006).
- ²³D. Saintillan, E. S. G. Shaqfeh, and E. Darve, "Stabilization of a suspension of sedimenting rods by induced-charge electrophoresis," *Phys. Fluids* **18**, 121701 (2006).
- ²⁴G. Yossifon, I. Frankel, and T. Miloh, "Symmetry breaking in induced-charge electro-osmosis over polarizable spheroids," *Phys. Fluids* **19**, 068105 (2007).
- ²⁵J. A. Levitan, S. Devasenathipathy, V. Studer, Y. Ben, T. Thorsen, T. M. Squires, and M. Z. Bazant, "Experimental observation of induced-charge electro-osmosis around a metal wire in a microchannel," *Colloids Surf., A* **267**, 122 (2005).
- ²⁶K. A. Rose, J. A. Meier, G. M. Dougherty, and J. G. Santiago, "Rotational electrophoresis of striped metallic microrods," *Phys. Rev. E* **75**, 011503 (2007).
- ²⁷S. Gangwal, O. J. Cayre, M. Z. Bazant, and O. D. Velev, "Induced-charge electrophoresis of metallodielectric particles," *Phys. Rev. Lett.* **100**, 058302 (2008).
- ²⁸J. Happel and H. Brenner, *Low Reynolds Number Hydrodynamics* (Prentice-Hall, Englewood Cliffs, NJ, 1965).
- ²⁹S. Kim and S. P. Karrila, *Microhydrodynamics: Principles and Selected Applications* (Butterworth-Heinemann, Boston, 1991).
- ³⁰D. J. Jeffrey, "Conduction through a random suspension of spheres," *Proc. R. Soc. London, Ser. A* **335**, 355 (1973).
- ³¹D. J. Jeffrey and Y. Onishi, "Calculation of the resistance and mobility functions for two unequal rigid spheres in low-Reynolds number flow," *J. Fluid Mech.* **139**, 261 (1984).
- ³²A. Z. Zinchenko, "An efficient algorithm for calculating multiparticle thermal interaction in a concentrated dispersion of spheres," *J. Comput. Phys.* **111**, 120 (1994).
- ³³M. Loewenberg and E. J. Hinch, "Numerical simulation of a concentrated emulsion in shear flow," *J. Fluid Mech.* **391**, 249 (1986).
- ³⁴C. Pozrikidis, *Boundary Integral and Singularity Methods for Linearized Viscous Flow* (Cambridge University Press, Cambridge, 1992).
- ³⁵C. Pozrikidis, "Three-dimensional oscillations of inviscid drops induced by surface tension," *Comput. Fluids* **30**, 417 (2001).
- ³⁶M. Washizu, "Precise calculation of dielectrophoretic force in arbitrary field," *J. Electrostat.* **29**, 177 (1992).
- ³⁷A. Biesheuvel and L. van Wijngaarden, "The motion of pairs of gas bubbles in a perfect fluid," *J. Eng. Math.* **16**, 349 (1982).
- ³⁸J. B. W. Kok, "Dynamics of a pair of gas bubbles moving through liquid," *Eur. J. Mech. B/Fluids* **12**, 515 (1993).
- ³⁹C. Pozrikidis, "Interception of two spheroidal particles in shear flow," *J. Non-Newtonian Fluid Mech.* **136**, 50 (2006).
- ⁴⁰The two effects described in this paper (DEP and ICEP interactions) both fall in a broader category of nonlinear motions arising as a result of symmetry breaking (both effects indeed disappear in the single sphere case). These also arise in other situations in which symmetries are broken, such as for isolated particles with asymmetric shapes (Refs. 20 and 22) or for isolated spherical particles in the vicinity of rigid boundaries (Ref. 11). In addition, other types of nonlinear effects may in some cases also result in qualitatively similar interactions, for example, the action of weak fluid inertia (Ref. 41).
- ⁴¹E. Yariv, "Inertia-induced electrophoretic interactions," *Phys. Fluids* **16**, L24 (2004).
- ⁴²E. Yariv and H. Brenner, "Near contact electrophoretic motion of a sphere parallel to a planar wall," *J. Fluid Mech.* **484**, 85 (2003).
- ⁴³E. Yariv and T. Miloh, "Electro-convection about conducting particles," *J. Fluid Mech.* **595**, 163 (2008).
- ⁴⁴M. Abramowitz and I. A. Stegun, *Handbook of Mathematical Functions with Formulas, Graphs, and Mathematical Tables* (Dover, New York, 1972).